







Atomistic simulations of α -Fe/Nd₂Fe₁₄B magnetic core/shell nanocomposites with enhanced energy product for high temperature permanent magnet applications

Cite as: J. Appl. Phys. **127**, 133901 (2020); <https://doi.org/10.1063/1.5126327>

Submitted: 01 September 2019 . Accepted: 13 March 2020 . Published Online: 01 April 2020

Sam C. Westmoreland , Connor Skelland , Tetsuya Shoji, Masao Yano, Akira Kato, Masaaki Ito, Gino Hrkac , Thomas Schrefl , Richard F. L. Evans , and Roy W. Chantrell 



View Online



Export Citation



CrossMark

ARTICLES YOU MAY BE INTERESTED IN

[Influence of disorder and surface roughness on the electrical and thermal properties of lithiated silicon nanowires](#)

Journal of Applied Physics **127**, 135101 (2020); <https://doi.org/10.1063/5.0002980>

[Evolving structure–property relationships in metals with nonequilibrium concentrations of vacancies](#)

Journal of Applied Physics **127**, 135901 (2020); <https://doi.org/10.1063/5.0004014>

Lock-in Amplifiers
Find out more today



 Zurich
Instruments



Atomistic simulations of α -Fe/Nd₂Fe₁₄B magnetic core/shell nanocomposites with enhanced energy product for high temperature permanent magnet applications

Cite as: J. Appl. Phys. **127**, 133901 (2020); doi: [10.1063/1.5126327](https://doi.org/10.1063/1.5126327)

Submitted: 1 September 2019 · Accepted: 13 March 2020 ·

Published Online: 1 April 2020



View Online



Export Citation



CrossMark

Sam C. Westmoreland,¹ Connor Skelland,² Tetsuya Shoji,³ Masao Yano,³ Akira Kato,³ Masaaki Ito,³ Gino Hrkac,² Thomas Schrefl,⁴ Richard F. L. Evans,^{1,a)} and Roy W. Chantrell¹

AFFILIATIONS

¹Department of Physics, The University of York, York YO10 5DD, United Kingdom

²College of Engineering, Mathematics and Physical Sciences, University of Exeter, Exeter EX4 4QF, United Kingdom

³Toyota Motor Corporation, Toyota City 471-8572, Japan

⁴Center for Integrated Sensor Systems, Danube University Krems, E 2700 Wiener Neustadt, Austria

^{a)}Author to whom correspondence should be addressed: richard.evans@york.ac.uk

ABSTRACT

Nd₂Fe₁₄B has generated significant interest since its discovery in the 1980s due to its impressive energy density, which makes it a prime candidate for use in permanent magnet applications. Its performance is known to suffer greatly at the high temperatures required for motor applications around 450 K. Core/shell nanocomposites provide a potential route to improve material performance by combining the highly anisotropic permanent magnet with a material with high moment and high Curie temperature. We have used an atomistic spin model to investigate the magnetic properties of Nd₂Fe₁₄B with α -Fe in a core/shell nanostructure. We find that at typical motor operating temperatures, increasing α -Fe content reduces the coercivity of the system while enhancing the saturation magnetization. The overall effect is that an improvement in BH_{\max} is seen with increasing α -Fe up to an optimal value of 70 vol. %. This property of core/shell nanostructures would make them a suitable substitute for pure Nd₂Fe₁₄B while simultaneously lowering the raw material cost of the permanent magnet component of high-performance motors.

Published under license by AIP Publishing. <https://doi.org/10.1063/1.5126327>

I. INTRODUCTION

Nd₂Fe₁₄B has attracted considerable interest since its discovery in the early 1980s^{1,2} due to its extremely high maximum energy product (BH_{\max}) at room temperature. This intrinsic property makes it an excellent choice of material for use in motors for electric vehicles and wind turbines. There are two main problems with the material however. The first is its low Curie temperature ($T_C = 585$ K). The second is the strong temperature dependence of the coercivity, which results in a rapid drop in BH_{\max} with increasing temperature. For use in high-performance permanent magnet applications, the magnet is required to maintain its performance at temperatures up to $T = 450$ K. A common solution to this problem is to dope the material with heavy rare-earth elements,

most often dysprosium. Dy doping results in better behavior at elevated temperatures; however, its use is unsustainable due to high cost and scarcity. The addition of Dy also results in a loss of saturation magnetization, which is detrimental to BH_{\max} .

A third obstacle is the theoretical limit placed on BH_{\max} for a given material, given by

$$BH_{\max} \leq \mu_0 M_s^2 / 4, \quad (1)$$

where M_s is the saturation magnetization. The expression gives the value for BH_{\max} corresponding to an ideal rectangular hysteresis loop. This puts a theoretical limit on the increasing trend in BH_{\max} observed over the past century,³ where improvement at each stage

has come about through the discovery of new materials. In the case of $\text{Nd}_2\text{Fe}_{14}\text{B}$, the theoretical limit is calculated to be $\sim 509 \text{ kJ m}^{-3}$, though in practice, the best current magnets have a maximum energy product of $\sim 350 \text{ kJ m}^{-3}$, and the prospect of discovering new materials going forward appears poor.⁴

Recent advancements in nanoscale fabrication techniques have opened the way for a new class of materials that combine hard and soft magnetic materials to produce so-called exchange-coupled nanocomposites, or *exchange spring* magnets,^{5–9} with high anisotropy provided by the hard phase and high saturation magnetization provided by the soft phase. In addition to having better overall magnetic properties than either constituent material, exchange spring magnets have the advantage of reducing the overall material cost by reducing the proportion of the expensive hard phase in favor of more cost-effective and readily available soft materials such as Fe or Co. Since first suggested by Kneller and Hawig in 1991,⁵ various theoretical predictions have suggested that their maximum energy product could be in the region of 950 kJ m^{-3} , which is remarkable when compared to what one could hope to achieve using only permanent magnets; however, this has not yet been realized experimentally.

Skomski and Coey (1993)⁴ predicted theoretically that in a bi-magnetic multilayer system comprised of $\text{Sm}_2\text{Fe}_{17}\text{N}_3$ as the hard phase and $\text{Fe}_{65}\text{Co}_{35}$ as the soft phase, a BH_{max} of 1 MJ m^{-3} could be achieved. Despite the great potential for improving BH_{max} using bi-component ferromagnetic materials, the majority of research has focused on FM/AFM or AFM/FM core/shell nanostructures^{10–13} for applications in magnetic recording and biomagnetism. However, recently, Liu *et al.* reported values of $360\text{--}440 \text{ kJ m}^{-3}$ for FeCo and Fe coated $\text{Nd}_2\text{Fe}_{14}\text{B}$ particles.¹⁴ It has been suggested that the reason for this disparity between experimental and predicted values might be that experiments have been carried out on randomly oriented particles.¹⁰

There are a number of methods used in the literature to treat exchange spring magnets computationally. Currently, the most common is based on the micromagnetics formalism,^{15–18} which approximates the magnetization of the system as a spatially continuous vector field. While applicable to larger nanocomposites, the micromagnetic formalism is unsuitable for studying very fine particles where finite size effects become important and at elevated temperatures where the local magnetic moments are no longer collinear, thereby breaking the principal assumption of a continuous variation of the magnetization implicit in the micromagnetic formulation.

In the current work, we have carried out a systematic investigation of the magnetic properties and performance of idealized core/shell nanostructures with soft/hard morphology, using $\text{Nd}_2\text{Fe}_{14}\text{B}$ for the hard phase shell and $\alpha\text{-Fe}$ for the soft phase core. The systems are modeled across a range of temperatures using an atomistic spin dynamics (ASD) model. The ASD approach is the most appropriate way to deal with interface effects and elevated temperatures, which form an important part of the current work. The paper is organized as follows. We first outline the basis of the ASD method, including the use of spin temperature rescaling (STR) to more accurately represent the temperature dependent magnetization of quantum magnets. We then present investigations of the temperature dependence of the magnetization, which demonstrate an important

enhancement of the magnetization of the hard phase via the exchange interaction with the $\alpha\text{-Fe}$ core. This is followed by a systematic investigation of the temperature dependences of the coercive field and the maximum energy product, where we show that there is an overall enhancement of the magnetic properties again due to the inter-phase exchange coupling.

II. METHOD

The atomistic spin model approximates the magnetic system as a discrete three-dimensional lattice of vectors representing atomic magnetic dipole moments. The moments are allowed to point in any direction in space, following the classical Heisenberg model. The energy is minimized at each site according to the spin Hamiltonian, which takes the form,

$$\mathcal{H} = -\frac{1}{2} \sum_{ij} J_{ij} \mathbf{S}_i \cdot \mathbf{S}_j - k_u \sum_i (\mathbf{S}_i \cdot \mathbf{e})^2 - \sum_i \mu_s \mathbf{S}_i \cdot \mathbf{H}_{\text{app}}. \quad (2)$$

The first term on the right-hand side is the Heisenberg form of the exchange energy, where \mathbf{S}_i and \mathbf{S}_j are the normalized atomic spin vectors on sites i and j , respectively, with $|\mathbf{S}| = 1$, and J_{ij} is the exchange integral between those sites. Here, J_{ij} is assumed to be isotropic and short ranged, truncated at nearest neighbor distance. The second term represents the anisotropy energy at site i . We assume here a uniaxial single-ion anisotropy, with k_u being the uniaxial anisotropy constant given in units of Joules per atom and \mathbf{e} being the easy-axis, which is assumed to lie along z . The third term gives the Zeeman energy, where \mathbf{H}_{app} denotes an externally applied field.

The calculation of the energy product of the system requires simulation of hysteresis loops. To do this, we model the spin dynamics of the system using the stochastic Landau–Lifshitz–Gilbert equation¹⁹ with Langevin dynamics used to incorporate stochastic thermal effects. The equation of motion for the spins applied at the atomic level²⁰ takes the form

$$\frac{\partial \mathbf{S}_i}{\partial t} = -\frac{\gamma}{1 + \lambda^2} [\mathbf{S}_i \times \mathbf{H}_{\text{eff}}^i + \lambda \mathbf{S}_i \times (\mathbf{S}_i \times \mathbf{H}_{\text{eff}}^i)], \quad (3)$$

where λ and γ are the *microscopic* Gilbert damping parameter (distinct from the usual Gilbert damping parameter in that extrinsic effects are included explicitly within the model²¹) and gyromagnetic ratio, respectively. The first derivative of the spin Hamiltonian with respect to the spin direction gives an effective field, which interacts with the spin at the given site. Thermal effects are included in the model in a natural way via a Langevin dynamics term, which is added to the effective field,

$$\mathbf{H}_{\text{eff}}^i = -\frac{1}{\mu_s} \frac{\partial \mathcal{H}}{\partial \mathbf{S}_i} + \Gamma(t) \sqrt{\frac{2\lambda k_B T}{\gamma \mu_s \Delta t}}, \quad (4)$$

where k_B is the Boltzmann constant, T is the temperature of the system, and Δt is the integration time step. $\Gamma(t)$ is a three-dimensional Gaussian distribution representing stochastic thermal fluctuations.

For calculating the equilibrium properties of the system, i.e., effects with rapid convergence to equilibrium, such as the

temperature dependence of the magnetization, it is optimal to use a Monte Carlo algorithm.^{21,22}

In the classical atomistic Heisenberg model, all spin directions are permitted for the localized spin vector, as opposed to an Ising model with a global quantization axis for the spins. This naturally describes spin waves but suffers from the classical approximation to the thermodynamic properties leading to an incorrect temperature dependence for the system magnetization at low temperatures.²³ One method of correcting this is to use the phenomenological STR method suggested by Evans *et al.*,²³ which results in good agreement with experiment by effectively reducing the strength of spin fluctuations in the simulated system, thereby approximating the true quantum nature of the heat bath. The approach uses an interpolation between low-temperature Bloch behavior and critical (Curie) behavior, such that the magnetization can be described by the Curie–Bloch equation,

$$m(\tau) = (1 - \tau^\alpha)^\beta, \quad (5)$$

where $\tau = T/T_c$, α is a phenomenological constant, and β is the critical exponent. β is assumed to be the same for the classical simulation and experiment. Setting $\alpha = 1$ (corresponding to the classical Heisenberg dependence of the magnetization), we can determine both β and T_c , which are constants. With these, we are able to perform a secondary fit to the experimental data to determine α . Using this method gives re-scaling constants $\alpha_{\text{Fe}} = 2.876$ ²³ and $\alpha_{\text{NdFeB}} = 1.756$,^{24,25} which we apply to the α -Fe and Nd₂Fe₁₄B sublattices, respectively, allowing the temperature dependence of the saturation magnetization and energy product of the composite system to be compared to experiment. This is important to accurately assess the changes in magnetic properties with temperature, not achievable with a simple classical model.

III. RESULTS

We have carried out a systematic investigation of the properties of core/shell Nd₂Fe₁₄B/ α -Fe nanoparticles. We first establish that the parameters for the isolated phases produce behavior consistent with experiment and previous atomistic calculations. Following this, we consider the effect of varying the relative proportions of the phases in the core/shell configuration on the temperature dependence of the saturation magnetization. This is then followed by an investigation of the hysteresis behavior of nanoscale systems.

A. Static magnetic properties and proximity effect

The temperature dependence of the magnetization of the two isolated phases is shown in Fig. 1. Here, we study the temperature dependent magnetization in the full temperature range from 0 K to $T > T_c$ to verify agreement with the experimental data for the shape of the $m(T)$ curve and the Curie point of the material. The system is first equilibrated with 10 000 Monte Carlo steps at each temperature (taking the final configuration from the previous temperature point) and then 100 000 averaging Monte Carlo steps are performed where statistical averages are calculated. The magnetization behaves as desired for both the Nd₂Fe₁₄B and α -Fe phases after re-scaling via the STR method. Fitting using the Curie–Bloch

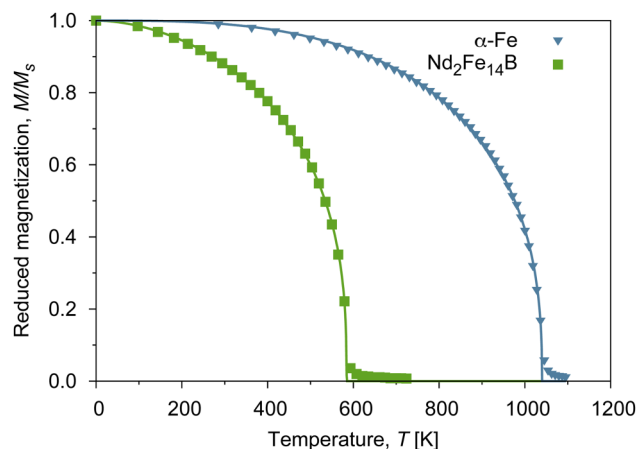


FIG. 1. Calculated temperature dependent magnetization for single-phase spherical nanoparticles of diameter 12 nm. The curves are fitted using Eq. (5), giving values for T_c of 584.3 K for Nd₂Fe₁₄B (experimental value 585 K²⁶) and 1040.0 K for α -Fe (experimental value 1041 K²⁷).

equation [Eq. (5)] gives values for T_c of 584.3 K and 1040.0 K for Nd₂Fe₁₄B and α -Fe, respectively, in agreement with previous atomistic simulations on the pure materials.^{23,25} Having aligned our model with the experimental parameters, we now investigate the temperature dependence of the composite nanoparticle properties.

First, we investigate the magnetization of the core/shell system, showing an important proximity effect arising from the polarization of the hard phase by the α -Fe core. The interfacial exchange between α -Fe and Nd₂Fe₁₄B is assumed to be the average of the two bulk exchange constants, providing strong coupling between the two components of the nanoparticles. We have calculated the temperature dependence of the magnetization as a function of the vol. % of α -Fe, using the Monte Carlo integration method as outlined in Sec. II. From Fig. 2, it can be seen that there is a clear enhancement of the saturation magnetization across the whole temperature range for increasing vol. % of α -Fe. Due to its higher T_c , the gradient of the magnetization curve for bulk α -Fe is much smaller at low temperatures than that of Nd₂Fe₁₄B, which will, in the exchange-coupled case, result in increased magnetization of the composite phase. The highlighted temperature region 300–450 K in Fig. 2 indicates the area of interest when considering electric vehicle motor applications. The enhancement effect is significant toward the high temperature end of this region, where Nd₂Fe₁₄B begins to de-magnetize as T approaches T_c for bulk Nd₂Fe₁₄B. The more thermally stable α -Fe phase acts to polarize the shell via the inter-phase exchange coupling. For high fractions of α -Fe, there is also a significant induced magnetization in the Nd₂Fe₁₄B phase even above the bulk Curie temperature, which suggests that such a composite structure may also be useful for high temperature applications. Interestingly, this is a consequence of the α -Fe being the inner material, leading to a large surface area coupled to a high T_c material. In the inverted case, a Nd₂Fe₁₄B core would have a much weaker inner magnetization that would likely have a lower magnetization above the Curie temperature.

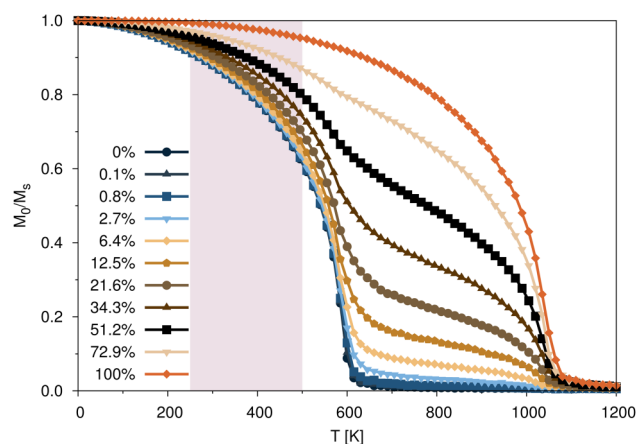


FIG. 2. The calculated saturation magnetization as a function of temperature for a 12 nm diameter soft/hard core/shell nanoparticle for varying vol. % of α -Fe. Though the curves do not follow the standard Curie–Bloch behavior, qualitatively it can be said that there is a clear increase in T_c with increasing α -Fe content, as well as improved magnetization retention across all temperatures considered. The highlighted region indicates the temperature domain generally relevant for automotive applications. The calculations used 10 000 equilibration and 100 000 averaging Monte Carlo steps at each temperature to ensure accurate statistical averages for the magnetization.

The extent of the polarization effect within the hard phase was investigated by calculating the magnetization of the particle as a function of the radial distance r from the center of the particle, shown schematically in Fig. 3. In the uncoupled case, one would

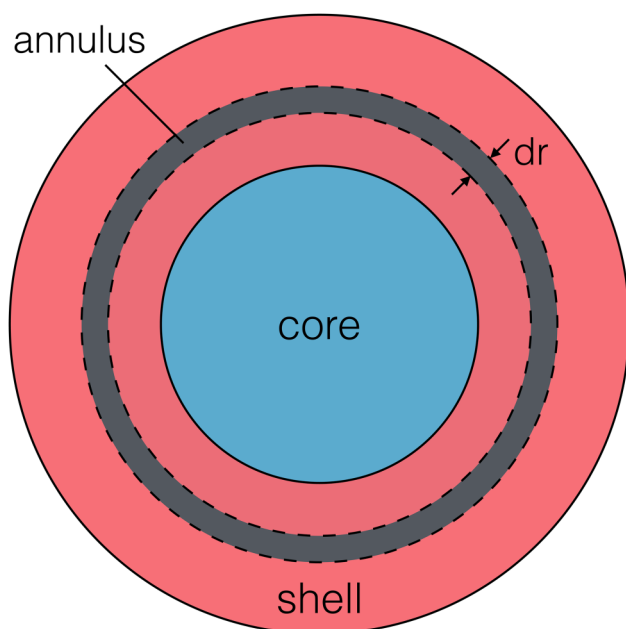


FIG. 3. Discretization of core/shell particle into series of annuli of constant width dr , with radius ranging from zero to radius of particle.

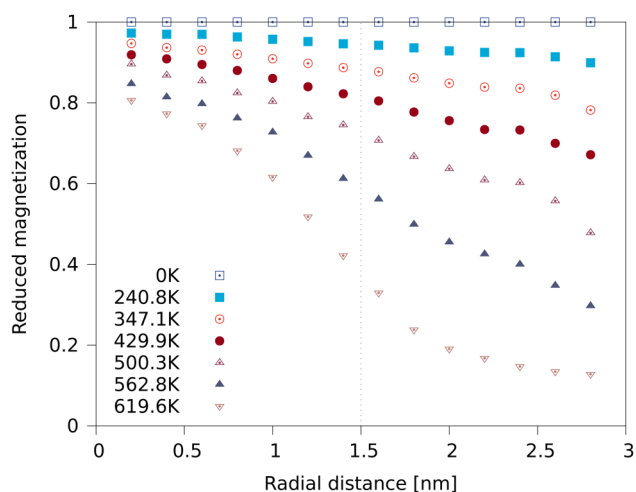


FIG. 4. The calculated magnetization as a function of radial distance from the particle center for soft/hard core/shell nanoparticles for varying volume percentage of α -Fe. The particle considered here is a 6 nm diameter sphere with the 3 nm core, so the core/shell interface is 1.5 nm from the center, indicated in the figure by the dotted line. The drop in magnetization between the core and the shell is predicted by Fig. 2, where, due to the lower Curie temperature and smaller α , for a given temperature, the magnetization is lower for smaller core volumes. The key point, however, is the gradient of the drop in magnetization, a result of the inter-phase exchange coupling, and it can be seen that the core polarizes the hard shell to a depth of ~ 0.5 nm.

expect a step-function change in the magnetization at the distance $r = r_c$, where r_c is the radius of the core. In the coupled case considered here, the calculations clearly show a gradual transition from the soft to the hard phase, with the gradient of $M(r)$ directly proportional to the coupling strength. This is an interesting effect, accessible experimentally and with direct implications for applications in systems based on nanoscale materials design. Figure 4 shows the results of the $M(r)$ calculation, which was done by dividing the particle into a discrete series of annuli, vectorially summing the atomic spins within each successive annulus and finally dividing by the number of spins found within the annulus. At low temperatures, both the α -Fe core and $\text{Nd}_2\text{Fe}_{14}\text{B}$ shell are highly ordered. The first feature to develop at intermediate temperatures is the reduction of the ordering at the particle surface. This is due to reduced surface coordination leading to missing exchange bonds. Surface spin fluctuations then cause a reduction in the surface magnetization compared to the inner regions of the particle. In general, the data show that there is a gradual and approximately linear transition between the higher magnetization of the soft core and the reduced magnetization of the hard shell. The polarization effect of the soft α -Fe core can be seen to penetrate the shell to a depth of ~ 0.5 nm, or 17% the thickness of the shell, providing an explanation for the enhancement effect seen in Fig. 2.

B. Hysteretic properties and energy product

We now proceed to investigate the hysteresis properties and energy product of the core/shell structure. While the composite system reduces the temperature dependence of the saturation

magnetization, a high energy product is dependent upon retaining a high coercivity. Since the Fe has a very low anisotropy, its addition will also lead to a reduction in the coercivity of the composite system. We proceed by investigating the coercivity as a function of temperature, followed by a study of the temperature dependence of the energy product as a function of the Fe vol. %. Figure 5 shows hysteresis loops at temperatures of 0 K and 300 K. The hysteresis loops for the composite system were generated using a field sweep rate of $6.0 \times 10^8 \text{ T s}^{-1}$ (real time), which equates to $\sim 24\,000$ steps per field point sweeping between 18.5 T and -18.5 T and a field increment of $3 \times 10^{-3} \text{ T}$. The computed hysteresis loops are at a much faster field rate than laboratory experiments, but are sufficiently slow to avoid the ballistic regime, where the magnetization is unable to equilibrate to the field direction.²² Our calculations should, therefore, closely approximate the intrinsic coercivity for an equivalent laboratory measurement of a single particle. Note that here we do not consider the rate dependence of coercivity due to thermal agitation over small energy barriers from the Sharrock equation, as the coercivities of the particles are relatively large.

The squareness of the loops suggests that a coherent rotation mechanism is at work, independent of the Fe vol. %, as expected due to the small particle size. It is shown that particles with increased Fe core size show much lower coercivity and also an enhanced moment. At elevated temperatures, the total moment is decreased, as is the coercive field.

The dependence of the coercive field of the nanoparticle on the fraction of $\alpha\text{-Fe}$ at zero temperature and room temperature is shown in Fig. 6. It can be seen that the coercive field decreases with increasing $\alpha\text{-Fe}$ fraction, with the most significant decrease seen at zero temperature. It is interesting to note that the reduction in coercivity with changing fractions of soft material is non-linear, which is a common feature of composite systems with different

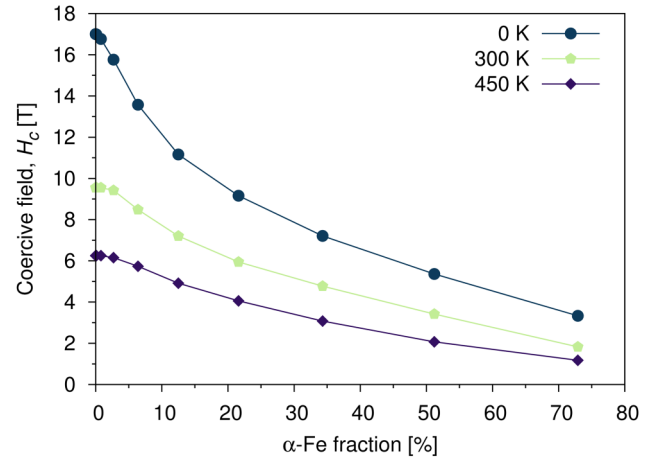


FIG. 6. Calculated coercive field as a function of vol. % of $\alpha\text{-Fe}$ at zero temperature, room temperature, and operating temperature of a permanent magnet motor.

magnetic properties.²⁸ Here, elevated temperatures reduce the non-linearity of the variation of coercivity, suggesting an increasing benefit for core-shell composite structures at elevated temperatures. For temperatures above 200 K, all particles with a fractional Fe content over 80% approach thermal instability, with a low coercivity ($< 2 \text{ T}$) and, therefore, unsuitable for motor applications. At 200 K, there is also an appreciable rounding of the hysteresis loop arising from thermal fluctuations within the local energy minimum: a factor which gives a further slight reduction in the energy product.

The loss of performance of $\text{Nd}_2\text{Fe}_{14}\text{B}$ in automotive applications is due in part to the loss of saturation magnetization at elevated operating temperatures. The polarization effect means that the advantages of adding Fe, in addition to the reduction of the Nd for cost reasons, are twofold. First, the Fe enhances the overall magnetization, giving rise to a potential increase in energy product (albeit offset by a reduction in coercivity). Second, the polarization of the $\text{Nd}_2\text{Fe}_{14}\text{B}$ by the Fe stabilizes the hard phase at elevated temperatures and thereby reduces the rate of reduction of the anisotropy field of the hard phase.

To determine the effectiveness of a permanent magnet in high-performance motor applications, we consider the quantity $(BH)_{\text{max}}$, or the maximum energy product, where BH is a scalar product between the induced magnetic flux density B and the internal magnetic field H_{int} . B is given by

$$B = \mu_0(M + H_{\text{int}}), \quad (6)$$

where M is the magnetization of the particle and H_{int} is the internal field, which is given by

$$H_{\text{int}} = \mu_0 H_{\text{ext}} - \frac{N_d}{4\pi} M, \quad (7)$$

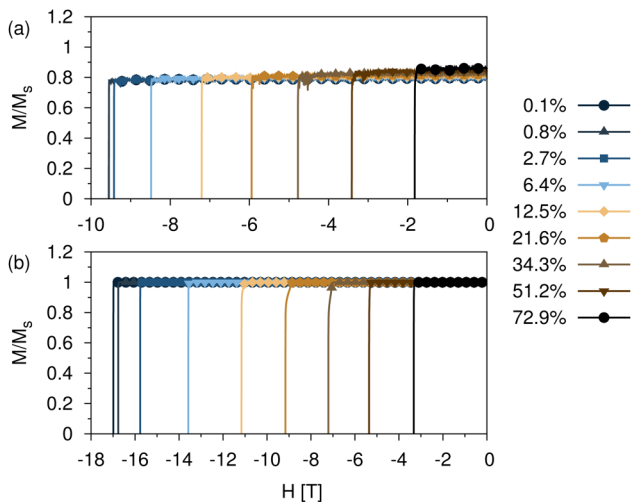


FIG. 5. Calculated de-magnetization curves for 12 nm diameter core/shell particles with varying vol. % of $\alpha\text{-Fe}$. (a) shows the variation of H_c for a system at 300 K and (b) at 0 K.

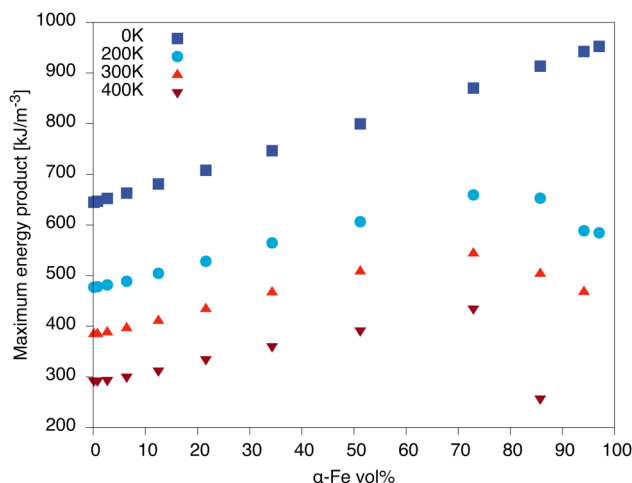


FIG. 7. Calculated maximum energy product of composite 6 nm nanoparticle for a range of temperatures. The temperature labels here refer to the simulation temperature. At finite temperatures, a steady increase is seen as a function of Fe core volume, which continues up to a threshold value of $\sim 70\%$, after which a rapid decline is seen. This suggests that for composite nanoparticles, in general, there is an ideal core size at which the maximum energy product may be optimized. At zero temperature, there does not appear to be a threshold value.

where $\mu_0 H_{\text{ext}}$ is the externally applied magnetic field and N_d is the demagnetizing factor, taken to be $4\pi/3$ for a sphere.²⁹ In the calculation of the BH product, we have assigned a composite magnetic moment to the particle, weighted according to the relative volumes of the two phases. In general, a larger magnitude of BH_{max} is desirable.

The quantitative effects on the maximum energy product are shown in Fig. 7. It is seen that, at finite temperatures, there is an optimal system composition at which the maximum energy product reaches a maximum. This is found to be $\sim 70\%$. After this point, a sharp drop in the maximum energy product is observed. The drop is a result of the decreasing thickness of the hard $\text{Nd}_2\text{Fe}_{14}\text{B}$ shell, which is the source of the high coercive field necessary to achieve a large energy product and also to stabilize finite sized particles. Above $\sim 70\%$ $\alpha\text{-Fe}$ content, the coercivity drops significantly, making the particles unsuitable for applications and also reducing the energy product. However, for lower concentrations of $\alpha\text{-Fe}$ there is a significant benefit of the composite structure at high operating temperatures of $T = 400\text{ K}$, where the BH_{max} is up to 30% larger than for the pure $\text{Nd}_2\text{Fe}_{14}\text{B}$ phase, giving a large boost to the performance of the magnet.

IV. CONCLUSIONS

Using a generic atomistic spin model, the hysteretic and thermodynamic properties of $\text{Nd}_2\text{Fe}_{14}\text{B}$ hard shell/ $\alpha\text{-Fe}$ soft core nanostructures were investigated, with the aim of finding a structure with improved properties, namely, improved magnetization retention at elevated temperatures and larger maximum energy product BH_{max} . We found an improvement in the total magnetization of the composite system with increased $\alpha\text{-Fe}$ content. It was shown

that this was a result of a deep-penetrating polarization effect by the soft iron core on the hard shell, thereby increasing the Curie temperature of the hard phase. This enhancement was shown to be offset by a drop in coercivity with increasing Fe content, which reduced much more rapidly for larger $\alpha\text{-Fe}$ volume fractions sizes. Subsequently, it was shown that the combination of these two effects resulted in an overall increase in the maximum energy product of the particle with increasing $\alpha\text{-Fe}$ content, up to a threshold value of $\sim 70\%$, after which it was found to decrease rapidly. Thus, it has been shown that in the future, the performance of $\text{Nd}_2\text{Fe}_{14}\text{B}$ permanent magnets could potentially be optimized by the addition of $\alpha\text{-Fe}$, up to a certain volume fraction, in the form of core/shell nanoparticles, provided the particle size is sufficiently small that the interface exchange interaction is significant. This effect is especially important for high temperature applications where the operating temperature approaches the Curie temperature of the hard $\text{Nd}_2\text{Fe}_{14}\text{B}$ phase, where $\alpha\text{-Fe}$ can improve the energy product by up to 30%. Significant challenges remain in material fabrication however and may require the use of materials with a less complex crystal structure than $\text{Nd}_2\text{Fe}_{14}\text{B}$, and magnets with the ThMn_{12} structure are quite promising.³⁰

ACKNOWLEDGMENTS

This work is based on the results obtained from the future pioneering program “Development of magnetic material technology for high-efficiency motors” commissioned by the New Energy and Industrial Technology Development Organization (NEDO). The use of computational facilities funded by the EPSRC Small items of research equipment at the University of York ENERGY (Grant No. EP/K031589/1) is gratefully acknowledged.

REFERENCES

- M. Sagawa, S. Fujimura, H. Yamamoto, Y. Matsuura, and K. Hiraga, *IEEE Trans. Magn.* **20**, 1584 (1984).
- D. Givord, H. S. Li, and J. M. Moreau, *Solid State Commun.* **50**, 497 (1984).
- N. Poudyal and J. Ping Liu, *J. Phys. D Appl. Phys.* **46**, 043001 (2012).
- R. Skomski and J. M. Coey, *Phys. Rev. B Condens. Matter* **48**, 15812 (1993).
- E. F. Kneller and R. Hawig, *IEEE Trans. Magn.* **27**, 3588 (1991).
- E. E. Fullerton, J. S. Jiang, and S. D. Bader, *J. Magn. Magn. Mater.* **200**, 392 (1999).
- R. Skomski, *J. Phys. Condens. Matter* **15**, R841 (2003).
- S. Bance, H. Oezelt, T. Schrefl, M. Winklhofer, G. Hrkac, G. Zimanyi, O. Gutfleisch, R. F. L. Evans, R. W. Chantrell, T. Shoji, M. Yano, N. Sakuma, A. Kato, and A. Manabe, *Appl. Phys. Lett.* **105**, 192401 (2014).
- S. Bance, J. Fischbacher, and T. Schrefl, *J. Appl. Phys.* **117**, 17A733 (2015).
- A. López-Ortega, M. Estrader, G. Salazar-Alvarez, A. G. Roca, and J. Nogués, *Phys. Rep.* **553**, 1–32 (2015).
- R. F. L. Evans, D. Bate, R. W. Chantrell, R. Yanes, and O. Chubykalo-Fesenko, *Phys. Rev. B* **84**, 092404 (2011).
- F. Dorfbauer, R. Evans, M. Kirschner, O. Chubykalo-Fesenko, R. Chantrell, and T. Schrefl, *J. Magn. Magn. Mater.* **316**, e791 (2007).
- S. D. Oberdick, A. Abdelgawad, C. Moya, S. Mesbahi-Vasey, D. Kepaptsoglou, V. K. Lazarov, R. F. L. Evans, D. Meilak, E. Skoropata, J. van Lierop, I. Hunt-Isaak, H. Pan, Y. Ijiri, K. L. Krycka, J. A. Borchers, and S. A. Majetich, *Sci. Rep.* **8**, 3425 (2018).
- S. Liu, A. Higgins, E. Shin, S. Bauser, C. Chen, D. Lee, Y. Shen, Y. He, and M. Q. Huang, *IEEE Trans. Magn.* **42**, 2912 (2006).

- ¹⁵T. Schrefl, J. Fidler, and H. Kronmüller, *Phys. Rev. B Condens. Matter* **49**, 6100 (1994).
- ¹⁶J. Kuma, N. Kitajima, Y. Kanai, and H. Fukunaga, *J. Appl. Phys.* **83**, 6623 (1998).
- ¹⁷H. Fukunaga and H. Nakamura, *IEEE Trans. Magn.* **36**, 3285 (2000).
- ¹⁸H. Fukunaga, R. Horikawa, M. Nakano, T. Yanai, T. Fukuzaki, and K. Abe, *IEEE Trans. Magn.* **49**, 3240 (2013).
- ¹⁹T. L. Gilbert, *IEEE Trans. Magn.* **40**, 3443–3449 (2004).
- ²⁰M. O. A. Ellis, R. F. L. Evans, T. A. Ostler, J. Barker, U. Atxitia, O. Chubykalo-Fesenko, and R. W. Chantrell, *Low Temp. Phys.* **41**, 705 (2015).
- ²¹R. F. L. Evans, W. J. Fan, P. Chureemart, T. A. Ostler, M. O. A. Ellis, and R. W. Chantrell, *J. Phys. Condens. Matter* **26**, 103202 (2014).
- ²²J. D. Alzate-Cardona, D. Sabogal-Suárez, R. F. L. Evans, and E. Restrepo-Parra, *J. Phys. Condens. Matter* **31**, 095802 (2019).
- ²³R. F. L. Evans, U. Atxitia, and R. W. Chantrell, *Phys. Rev. B Condens. Matter* **91**, 144425 (2015).
- ²⁴R. F. L. Evans, A. Naden, S. Westmoreland, R. Cuadrado, M. Probert, T. Shoji, M. Yano, A. Manabe, G. Hrkac, T. Schrefl, D. Givord, and R. W. Chantrell “Atomistic simulation of temperature dependent properties of Nd₂Fe₁₄B” (unpublished) (2020).
- ²⁵Q. Gong, M. Yi, R. F. L. Evans, B.-X. Xu, and O. Gutfleisch, *Phys. Rev. B* **99**, 214409 (2019).
- ²⁶J. Herbst and J. Croat, *J. Magn. Magn. Mater.* **100**, 57 (1991).
- ²⁷F. Cardarelli, *Materials Handbook: A Concise Desktop Reference* (Springer Science & Business Media, 2008).
- ²⁸W. J. Fan, R. F. L. Evans, Y. Hancock, and R. W. Chantrell, *J. Appl. Phys.* **109**, 07B752 (2011).
- ²⁹D. J. Griffiths and R. College, *Introduction to Electrodynamics* (Prentice Hall, Upper Saddle River, NJ, 1999), Vol. 3.
- ³⁰C. Skelland, T. Ostler, S. C. Westmoreland, R. F. L. Evans, R. W. Chantrell, M. Yano, T. Shoji, A. Manabe, A. Kato, M. Ito, M. Winklhofer, G. Zimanyi, J. Fischbacher, T. Schrefl, and G. Hrkac, *IEEE. Trans. Magn.* **54**, 2103405 (2018).